The Journal of Experimental Biology 216, 2833-2842

doi:10.1242/jeb.085118

RESEARCH ARTICLE

X-ray motion analysis of the vertebral column during the startle response in striped bass, *Morone saxatilis*

B. N. Nowroozi* and E. L. Brainerd

Department of Ecology and Evolutionary Biology, Brown University, 80 Waterman Street, Box G-W, Providence, RI 02912, USA

*Author for correspondence at present address: Center for Advanced Surgical and Interventional Technology (CASIT), Department of Bioengineering, University of California, Los Angeles, CA 90095, USA (bnowroozi@ucla.edu)

SUMMARY

Whole-body stiffness has a substantial impact on propulsive wave speed during axial undulatory locomotion in fishes. The connective tissues of the vertebral column may contribute to body stiffness, but without mechanical and kinematic analysis it is unclear whether the *in vivo* range of motion of intervertebral joints (IVJs) is great enough to stress IVJ tissues, thus generating stiffness. The present study used 2D videoradiography and 3D X-ray reconstruction of moving morphology (XROMM) to quantify vertebral kinematics during the startle response in striped bass (*Morone saxatilis*). X-ray video revealed two distinct patterns of bending: pattern I begins in the abdominal region and then proceeds to maximum IVJ angles in the caudal region, whereas pattern II begins in the cervical region and proceeds to maximum IVJ angles in the abdominal and then the caudal joints. In pattern II bends, the cervical joints exhibit a greater *in vivo* range of motion than previously reported in other species. XROMM analysis of caudal IVJs suggests primarily lateral bending: mean axial and dorsoventral rotations were less than 2 deg and inconsistent across 51 sequences analyzed from five individuals, whereas mean maximum lateral bending angles were 10.4±3.57 deg. These angles, combined with previous investigations of mechanical properties, reveal that the maximum angles all occur within the neutral zone of bending, indicating that little stress is experienced about the joint. This suggests that the IVJs of striped bass are quite compliant and likely do not contribute significantly to whole-body stiffness or elastic recoil during swimming *in vivo*.

Supplementary material available online at http://jeb.biologists.org/cgi/content/full/216/15/2833/DC1

Key words: intervertebral joints, escape response, kinematics, stiffness, swimming, XROMM.

Received 10 January 2013; Accepted 27 March 2013

INTRODUCTION

Body stiffness is thought to impact locomotor performance in fish by increasing the speed of propulsive wave propagation and, ultimately, thrust (Wainwright et al., 1978; Long et al., 1994; Long and Nipper, 1996; McHenry et al., 1995; Long et al., 1996; Long, 1998; Long et al., 2002). While a variety of elements likely contribute to whole-body stiffness, it has been hypothesized that the vertebral column contributes passive stiffness to the body, thereby impacting thrust and possibly swimming energetics (Rockwell et al., 1938; Wainwright et al., 1978; Videler, 1993;Westneat et al., 1993; Long et al., 1994; McHenry et al., 1995; Long et al., 1996; Long, 1998; Long et al., 2002).

Specifically, it has been suggested that stiffness associated with the vertebral column is derived from vertebral centra and intervertebral joint (IVJ) tissues (Rockwell et al., 1938; Symmons, 1979; Long et al., 2002; Long et al., 2004). As the body bends during swimming, the vertebral centra and IVJ tissues are thought to resist compressive and tensile loading, thereby increasing body stiffness and possibly storing elastic energy (Rockwell et al., 1938; Nursall, 1958; Fierstine and Walters, 1968; Symmons, 1979; Hebrank, 1982; Videler, 1993; McHenry et al., 1995; Schmitz, 1995; Long et al., 2002; Long et al., 2004). This hypothesis assumes that as the vertebral column bends laterally, the IVJ tissues develop sufficient stress to have an impact on body stiffness and elastic energy storage. To test this hypothesis, mechanical testing must be combined with IVJ kinematics to determine whether appreciable stress is developed in the IVJ tissues at bending angles that are within the range of *in vivo* lateral bending angles.

Our recent study *in vitro* of the lateral bending mechanics of the vertebral column in striped bass, *Morone saxatilis*, revealed that the vertebral column is highly compliant, and therefore may not contribute significantly to whole-body stiffness (Nowroozi and Brainerd, 2012). That investigation of the IVJ tissue mechanics identified large neutral zones of bending, defined as the range over which a spinal segment moves freely without measurable resistance (Fig. 1) (Wilke et al., 1998; Long et al., 1996; Nowroozi and Brainerd, 2012). In the striped bass, these neutral zones of vertebral bending showed a range of up to 15 deg in lateral bending before appreciable force resisted the angular displacement. These results suggest that the IVJs of striped bass are highly compliant up to 15 deg of lateral bending, creating a neutral zone range beyond which stress begins to develop about the IVJ. While these neutral zones have not been seen in all species tested (Hebrank, 1982; Hebrank et al., 1990), they are not unique to striped bass (Long et al., 1996), and they have been identified in mammals as well (Gal, 1993a; Gal, 1993b; Panjabi et al., 2001; Kettler et al., 2004; Rousseau et al., 2007).

The presence of a large neutral zone of bending suggests that the contribution of the vertebral column to stiffness and energy efficiency may be insignificant. Given that very little stress is developed while the IVJ operates within the neutral zone, the

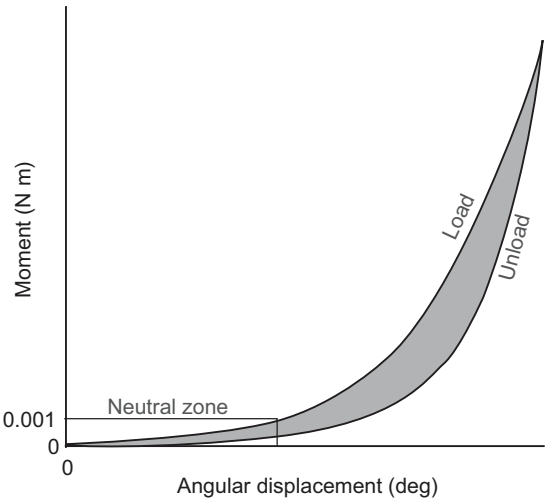

Fig. 1. Moment–angle curve (diagrammatic). The angular displacement refers to lateral bending from a straight position, and the neutral zone of bending is defined here as ranging from 0 deg to the angle at which the moment exceeds 0.001 N m (modified from Nowroozi and Brainerd, 2012).

vertebral and IVJ tissues can only contribute to angular stiffness if these vertebral segments bend beyond the 15 deg reported. However, 15 deg of lateral bending is greater than the lateral bending angles estimated based on the body curvature of a variety of species in previous studies (Jayne and Lauder, 1995; Brainerd and Patek, 1998; Donley and Dickson, 2000; Horner and Jayne, 2008). The species studied in these previous investigations exhibited maximum lateral bending angles across all IVJs along the length of the vertebral column, ranging between ~3 and 10 deg. While striped bass were not investigated in these previous studies, this range of angles is substantially lower than the 15 deg neutral zone reported for striped bass (Nowroozi and Brainerd, 2012).

In addition, previous estimates of IVJ bending *in vivo* indicate significant variation in the maximum lateral bending angle along the vertebral column from cranial to caudal (Jayne and Lauder, 1995; Brainerd and Patek, 1998; Donley and Dickson, 2000; Horner and Jayne, 2008). Across several species, these studies show lateral bending of up to 2 deg per IVJ in the cervical region, 5 deg in the abdominal region and 10 deg in the caudal region, with some species such as the largemouth bass (Jayne and Lauder, 1995) exhibiting larger angles compared with the kawakawa tuna, chub mackerel and African lungfish (Donley and Dickson, 2000; Horner and Jayne, 2008). This regional variation in lateral bending angles suggests that each IVJ, if bending beyond its neutral zone, will contribute differently to the whole-body stiffness of the fish. Thus, when considered along the length of the vertebral column, each individual joint must bend beyond its neutral zone to generate stiffness, and any axial variation in IVJ neutral zone and maximum IVJ bending will result in a variation in locomotor function along the length of the fish.

In fact, variation in neutral zone range was found during *in vitro* mechanical testing in the three regions of the vertebral column (cervical, abdominal and caudal) in striped bass (Nowroozi and Brainerd, 2012). The cervical joints exhibited a mean neutral zone range of up to 11.9 deg, while the abdominal and caudal joints demonstrated mean neutral zone ranges of up to 9.6 and 15.2 deg, respectively. Variation in the neutral zone in different regions of the vertebral column suggests that the abdominal joints could potentially contribute the most to overall body stiffness, followed by the cervical and then caudal joints. In addition, the abdominal joints were shown to have the greatest angular stiffness and most restricted range of motion compared with the cervical and caudal joints when these IVJs were bent beyond the neutral zones of bending (Nowroozi and Brainerd, 2012). This variation in IVJ mechanics across different regions of the vertebral column suggests that variation in stiffness and energy storage capabilities will impact regional kinematics and performance differently along the length of the fish. Therefore, the extent to which these vertebral segments contribute to whole-body stiffness, and swimming energetics, remains unclear without knowledge of accurate *in vivo* vertebral kinematics that can quantify the magnitude of bending that the IVJs undergo.

Thus, in the present study we examined the kinematics of the vertebral column and combined these data with previously reported morphological and mechanical data from a single species, *M. saxatilis* (Nowroozi et al., 2012; Nowroozi and Brainerd, 2012). We used videoradiography to investigate the 2D lateral bending kinematics of the vertebral column of striped bass during *in vivo* swimming. We investigated the regional differences in lateral bending angles attained throughout the startle response between the cervical (vertebrae 1–4), abdominal (vertebrae 5–12) and caudal (vertebrae 13–23) regions identified in the previous morphological study (Nowroozi et al., 2012). We quantified the range of motion and maximum angles attained along the length of the vertebral column and discuss these data relative to the predictions based on morphology and mechanics. These data offer a clear understanding of where along the force–displacement curve the IVJs operate *in vivo*, providing a glimpse of the energetics of the system, and helping to discern the contribution of each region of the vertebral column to whole-body stiffness and to swimming performance.

In addition to lateral bending of IVJs, the tissues of the vertebral column could potentially contribute to body stiffness and elastic energy storage by resisting axial and dorsoventral rotations during locomotion. While it is apparent from gross observation that the fish vertebral column bends laterally during body–caudal fin swimming, it is not clear whether other rotations or translations occur at the level of the individual IVJs. Experimental analyses of the caudal fin stroke of both bluegill sunfish (*Lepomis macrochirus*) and sturgeon (*Acipenser transmontanus*) have revealed asymmetries in motion between the dorsal and ventral lobes, suggesting axial rotation about the caudal vertebral column (Lauder, 2000). Thus, similar to the stresses associated with lateral bending, these axial rotations could develop appreciable stress in the IVJ tissues, thereby contributing to body stiffness. However, because of the deep position of the vertebral column, it has been difficult to quantify 3D *in vivo* vertebral kinematics.

Therefore, in supplement to the 2D investigation, in the present study we attempted to undertake the first investigation into the 3D kinematics of the vertebrae of fish to quantify any axial or dorsoventral rotation that may occur during *in vivo* swimming. We used X-ray reconstruction of moving morphology (XROMM) (Brainerd et al., 2010) to investigate the 3D kinematics of one vertebra–joint–vertebra segment in the caudal region of striped bass during the startle response. XROMM data can potentially determine whether substantial dorsoventral or axial rotation occurs at the level of the IVJs, leading to additional stress and contributing to whole-body stiffness.

MATERIALS AND METHODS

Animals

Eight striped bass, *M. saxatilis* (Walbaum), were obtained from the Susquehanna Aquaculture fish hatchery (York Haven, PA, USA).

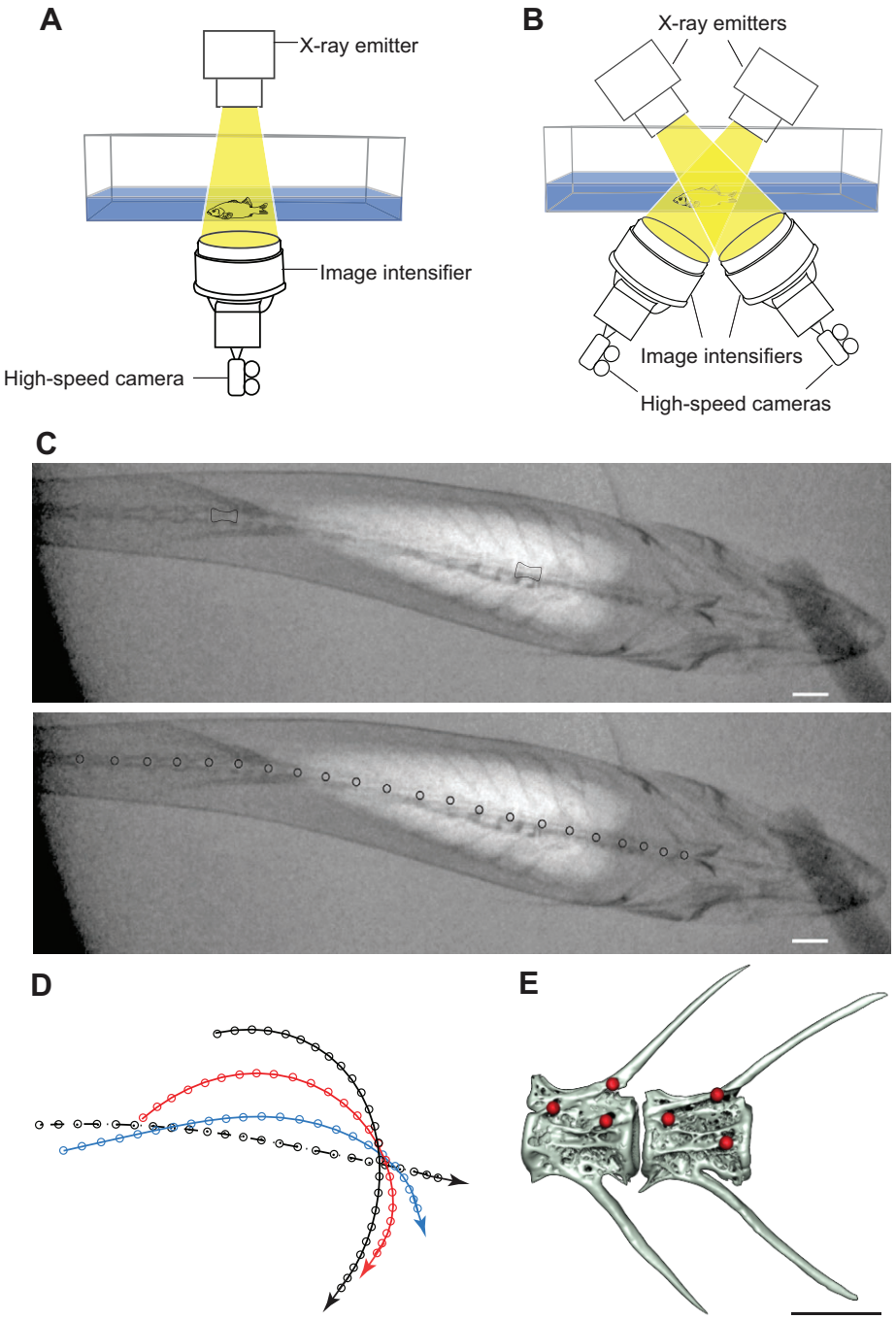

Fig. 2. X-ray motion analysis methods. Diagram of the experimental setup for (A) the 2D investigation and (B) the 3D XROMM investigation. The aquarium is 161 cm long, the water is 10 cm deep and the fish is about 30 cm long. High-speed, X-ray videos were recorded at 500 frames s^{-1}. (C) Dorsoventral view X-ray images of the vertebral column. Black outlines indicate one abdominal vertebra and one caudal vertebra. Black circles indicate the points digitized on the dorso-anterior aspect of each centrum. Scale bar, 10 mm. (D) Typical plots of raw *x*- and *y*-coordinates of vertebral centra (circles) and the planar curve fitted to those raw data (lines) for four time points during one sequence. The black dashed line is prior to movement, the blue line is during stage 1, the red line is at the deepest bend of the body, and the black solid line is during stage 2. Arrows indicate the orientation of the head. (E) Polygonal mesh surface models of vertebrae showing placement of the surgically implanted markers (red spheres) in one representative individual for XROMM study. The markers are 1 mm diameter tantalum spheres attached to 0.25 mm steel posts. The posts were implanted in the bone of the centra, such that the spheres lay just outside the centra. Scale bar, 10 mm.

Standard length of all eight fish was ~30 cm. Striped bass were chosen because of their relatively non-specialized vertebral morphology and their vertebral number. Striped bass have relatively few vertebrae for their body size. A comparable sized carp or trout has ~35 and 65 vertebrae, respectively (Nelson, 1994). Because the striped bass has only 24 vertebrae, each centrum has a greater length, resulting in a greater magnitude of bending at the IVJs (Nowroozi et al., 2012).

The fish were housed in a 300 gallon (~1150 l) circular aquarium at 19–22°C. Experiments were performed in a rectangular, acrylic tank (161×61×38 cm) filled to a depth of 10 cm such that the startle response was performed largely within the horizontal plane. In both the 2D and 3D investigations, the startle response was chosen for study because this escape behavior results in the largest magnitude of body bending along the length of the fish, thus generating the largest *in vivo* vertebral rotations and translations. The startle response was initiated by thrusting a dowel in close proximity to the head of the fish. All behaviors began from a stationary position and were performed at least 4 cm away from the walls of the experimental aquarium. Only those startle responses that exhibited the greatest magnitudes of whole-body bending, defined by the proximity of the snout to the tail, were used. All animal care and use procedures were approved by the Brown University Institutional Animal Care and Use Committee (protocol 0811088).

X-ray system

Each videoradiography system was composed of one Varian model G-1086 X-ray tube (Varian Medical Systems, Palo Alto, CA, USA),

one EMD technologies model EPS 45-80 X-ray generator (EMD technologies, Saint-Eustache, QC, Canada), and one Dunlee model TH9447QXH590 image intensifier (Philips Healthcare, Andover, MA, USA), 40 cm in diameter. The image intensifiers were fitted with Phantom v10 high-speed digital video cameras (Vision Research, Wayne, NJ, USA) to attain high-speed videoradiography (Fig. 2A,B). All sequences were filmed at 500 frames s^{-1} with an exposure time of 500 μs (see supplementary material Movie 1).

Data collection and processing

2D investigation

In the 2D lateral bending investigation, one fluoroscopy system was used to capture a dorsoventral view of the startle response in three fish (Fig. 2A,C). For all sequences, 70 kV and 320 mA provided the best possible clarity of the vertebral column. A total of 16 trials were analyzed with at least five trials per individual.

For each individual, the length of each vertebral centrum and IVJ was measured using ImageJ software (NIH). These measurements were taken from a single frame of video in which the fish was at rest in an unbent position. Next, using XrayProject software (Brainerd et al., 2010) in MATLAB (The Mathworks, Natick, MA, USA), the dorso-anterior aspect of each vertebral centrum was marked in each frame of video for every sequence (Fig. 2C; digitizing precision was measured to be 0.11 mm).

Given these *x*- and *y*-coordinates for each vertebral centrum, the radius of curvature of the vertebral column was calculated for each axial position. To this end, the vertebral column was treated as a planar curve (α) that can be evaluated from cranial to caudal such that:

$$\alpha(p) = \left(f(p), g(p)\right), \quad (1)$$

where p is the axial position of a particular vertebra, $f(p)$ is the x-coordinate of that vertebra and $g(p)$ is the y-coordinate of the same vertebra. The functions f and g were generated by fitting a quintic smoothing spline to the raw x- and y-coordinates in each frame using MATLAB. Fig. 2D shows four frames in time from one video sequence with the raw x- and y-coordinates (circles) for each vertebra and the resulting curve $\alpha(p)$ (lines) approximating the length of the vertebral column.

Using these two functions, the instantaneous radius of curvature (R) of the vertebral column was calculated at each axial position for each frame of video using the following differential geometric equation (Gray, 1993):

$$R = \frac{\left(f'^2(p) + g'^2(p)\right)^{3/2}}{\left(f'(p) \times g''(p)\right) - \left(g''(p) \times f''(p)\right)}, \quad (2)$$

where f is the function given by the spline fitted to the x-coordinates for that frame, and g is the function given by the spline fitted to the y-coordinates for the same frame. Given the radius of curvature at each body segment, the angle of bending between each pair of vertebrae was calculated as:

$$\Theta = \frac{S}{R}, \quad (3)$$

where S is the arc length taken as the sum of the lengths of the anterior vertebral centrum, the following IVJ and the posterior vertebral centrum. These calculations were performed for each frame of video.

3D XROMM investigation

Prior to data collection, surgical marker implantation was performed for each individual (Fig. 2E). Each fish was anesthetized *via* immersion in tricaine methanesulfonate (MS-222, 0.1 g l^{-1}) until opercular gilling had slowed substantially (1–2 min^{-1}). The fish was positioned on a surgical platform and a peri-operative dose of enroflaxacin (10 mg kg^{-1}; Baytril, Bayer Corporation, Morristown, NJ, USA) was administered intramuscularly (Lewbart and Harms, 1999; Govett et al., 2004; Harms, 2005).

An incision (~2.0–3.0 cm in length) was made posterior to the second dorsal fin, and immediately dorsal to the lateral line of the fish. Once the incision had been made, the two vertebrae were exposed using tissue spreaders, and a 0.24 mm hand-drill was used to drill three holes into each vertebra: one on the dorso-anterior aspect of the vertebra, one on the dorso-posterior aspect of the vertebra and one at the base of the neural spine. Care was taken during drilling not to puncture the joint cavity. A 0.25 mm diameter post with a spherical tantalum marker of 1 mm diameter attached was then manually pushed into the drilled hole such that each vertebra was marked with three tantalum markers (Fig. 2E). The vertebrae marked were always in the caudal region, and were typically vertebrae 19–20 or 20–21. The incision was sutured using sterile synthetic absorbable polydioxanone monofilament suture (5-0, Ethicon, Sommerville, NJ, USA), and a post-operative dose of butorphanol (0.4 mg kg^{-1}) was administered intramuscularly (Harms, 2005). The fish was returned to an 80 gallon (~300 l) 122×46×53 cm tank where it was quarantined and allowed to recover until normal swimming and feeding behavior resumed (~7–10 days).

In the 3D XROMM investigation, two fluoroscopy systems were used (Fig. 2B). The systems were oriented such that the angle between the two image intensifiers was ~120 deg and the angle between the X-ray beams was ~60 deg. All sequences were imaged at 100 kV and 200 mA. Appropriate calibration cube images and undistortion grid images were also acquired (Brainerd et al., 2010). A total of 51 sequences were analyzed with a minimum of nine sequences per individual for five individuals.

Fish were killed immediately after data collection and CT scanned to generate models of bones and markers for XROMM analysis (Brainerd et al., 2010). Scans were acquired with a helical medical scanner (Philips Medical Systems, Best, The Netherlands) at 1024×1024 image resolution, a field of view size of 25 cm, and a slice thickness of 0.625 mm. Scans were imported into Amira 4.0 3D visualization software (Mercury Computer Systems, Berlin, Germany). 3D polygonal mesh models of bone markers and vertebrae were generated in Amira (Fig. 2E).

Videos were digitized manually to obtain *xyz*-coordinates for each marker, and filtered using a Butterworth filter at a cut-off frequency of 25 Hz. Rigid body transformations were calculated using XrayProject software (Brainerd et al., 2010) in MATLAB (The Mathworks). The 3D bone and marker models were imported into Maya animation software (Autodesk, San Rafael, CA, USA) where centroids of each marker were calculated. The rigid body transformations were then applied to the bone models based on the movements of the markers to generate an XROMM animation of two vertebrae (Brainerd et al., 2010). Animations using both raw and filtered *xyz*-coordinates were generated.

Data analysis

2D investigation

The startle response has been previously defined by three kinematic stages: a preparatory stage, a propulsive stage and a variable stage when the fish glides or swims away (Weihs, 1973). We chose three points in time during the startle response to compare the pattern of bending throughout the behavior across sequences. We defined our second point in time as the frame of deepest body bending, when

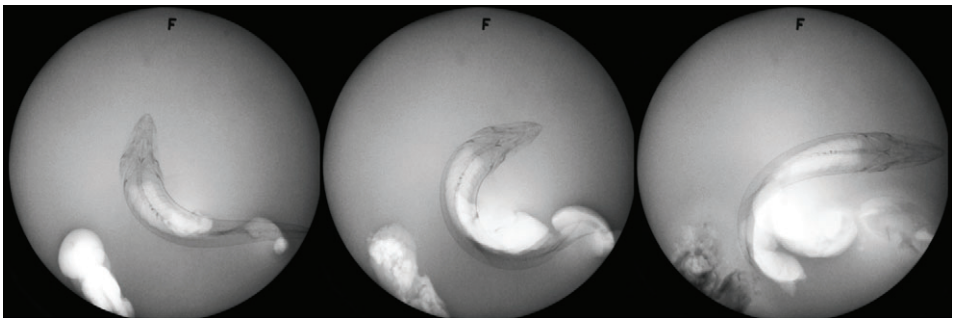

Fig. 3. Three frames of X-ray video showing the three points in time used to investigate the pattern of bending for each startle response. Time 1 corresponds to the middle of stage 1 of the startle response, time 2 corresponds to the transition between stage 1 and stage 2, and time 3 corresponds to the middle of stage 2. The brighter areas of overexposure are indicative of a change in water depth resulting from the movement of water due to the visual stimulus (lower left corner) and the movement of the fish.

the snout of the fish is closest to the tail. Using this time point as a reference, we defined the first time point as the frame that occurs halfway between the first frame of movement and the second time point. Similarly, we defined the third time point as the frame halfway between the second point and the frame in which the fish has straightened its body. Therefore, the first time point occurs during stage 1 of the startle response; the second time point corresponds to the transition between stage 1 and stage 2; finally, the third time point occurs during stage 2 of the startle response (Fig. 3). We then compared the mean angle of bending at each joint position for the three time points across all sequences.

Next, we calculated the maximum angle of bending attained at each IVJ throughout each sequence. The maximum angle attained for each joint represents the greatest degree of lateral bending at that axial position. Assuming that the fish are bending to their greatest overall body curvature during the startle responses that we analyzed, these values approximate the *in vivo* range of motion for each joint.

The effect of axial region on maximum angle of bending was tested using a nested ANOVA with individual as a nested factor. The differences between pairs of regions were tested *post hoc* using Tukey HSD multiple comparisons based on least-squared means. The vertebral column was divided into cervical (vertebrae 1–4), abdominal (vertebrae 5–12) and caudal (vertebrae 13–23) regions based on a previous analysis of anatomy (Nowroozi et al., 2012). All statistical results were interpreted using a Bonferroni correction to a significance level of 0.0166. Statistical analysis was performed using JMP software (version 8.0.1, SAS Institute, Cary, NC, USA).

3D XROMM investigation

To describe the 3D movement of one caudal vertebra relative to an adjacent vertebra, we created a joint coordinate system (JCS) in Maya (Brainerd et al., 2010). When the fish was in a straight posture (zero position for the JCS), the *z*-axis (blue) was oriented dorsoventrally to intersect with the neural and hemal spines of the anterior vertebrae, the *y*-axis (green) was oriented along the longitudinal axis of the fish through the amphicoels of both vertebrae, and the *x*-axis (red) was orthogonal to the *z*- and *y*-axes. The origin of the JCS was placed in the center of the joint, midway between the dorsal and ventral rims and left and right rims of the amphicoelous centra. In this way, mediolateral shear, axial translation and dorsoventral shear of the IVJ can be measured as translations along the *x*-, *y*- and *z*-axes, respectively. Likewise, dorsoventral bending, axial rotation and lateral bending can be measured as rotations about the *x*-, *y*- and *z*-axes, respectively. The rotation order hierarchy was *zyx*, and we set *z* to be lateral bending, the largest expected rotation. Sign convention for rotations is given by the right-hand rule, such that positive dorsoventral bending corresponds to a ventral rotation, positive axial rotation corresponds to a clockwise rotation of a posterior vertebra relative to an anterior vertebra (when viewed from the tail), and positive lateral bending corresponds to a bend to the right side of the fish. Animations for each of the 51 sequences were rendered and the 6 degrees of freedom kinematics were measured throughout each animation.

To compare bending across sequences and individuals, the portion of the behavior analyzed, the polarity of lateral bending and the polarity of axial rotation had to be consistent. As the startle response is a highly variable and non-cyclic behavior, we could not normalize the timing of the behavior in a repeatable manner. Thus, for each sequence we analyzed from the first frame of movement to 10 frames after the frame of peak bending at the marked vertebrae. This portion of the behavior captures stage 1, the transition between stage 1 and stage 2, and the portion of stage 2 where the marked vertebrae are bent maximally. In addition, to convert all sequences to 'right-hand' turns, all lateral bending and axial rotation measurements from sequences where the fish laterally bent concave to its left were multiplied by −1. The dorsoventral bending was not rectified because we do not expect differences in dorsoventral bending to be correlated to the handedness of the startle response.

To assess the precision of our aquatic experimental conditions, we used the variation in pairwise intermarker distance for markers implanted into the same vertebra (Brainerd et al., 2010). We measured 306 sets of pairwise intermarker distance from 51 raw (unfiltered) sequences. In addition, we measured 24 sets of pairwise intermarker distance from four raw sequences of a stationary fish in an attempt to characterize the effect of motion in the aquatic environment on the precision of the system. Finally, to estimate the resolution of the 6 degrees of freedom data, we quantified the root-mean square deviation (RMSD) for four stationary sequences relative to their means. As the fish are stationary, we expected these RMSD numbers to be zero. Deviations from zero will determine the translational and rotational resolution of XROMM in the current configuration.

RESULTS

2D lateral bending kinematics

The results of this 2D study reveal two distinct patterns of lateral bending during the startle response in *M. saxatilis* (Figs 4, 5). In both cases, bending during the startle response occurs as a traveling wave from cranial to caudal. In addition, there are ~10–15 IVJs (out of 24) that undergo substantial bending at any given moment during the behavior.

The first pattern of bending begins in the abdominal region, approximately at IVJs 7–10 (Fig. 4A). When the fish reaches its deepest overall body curvature, at time 2, the wave of bending has

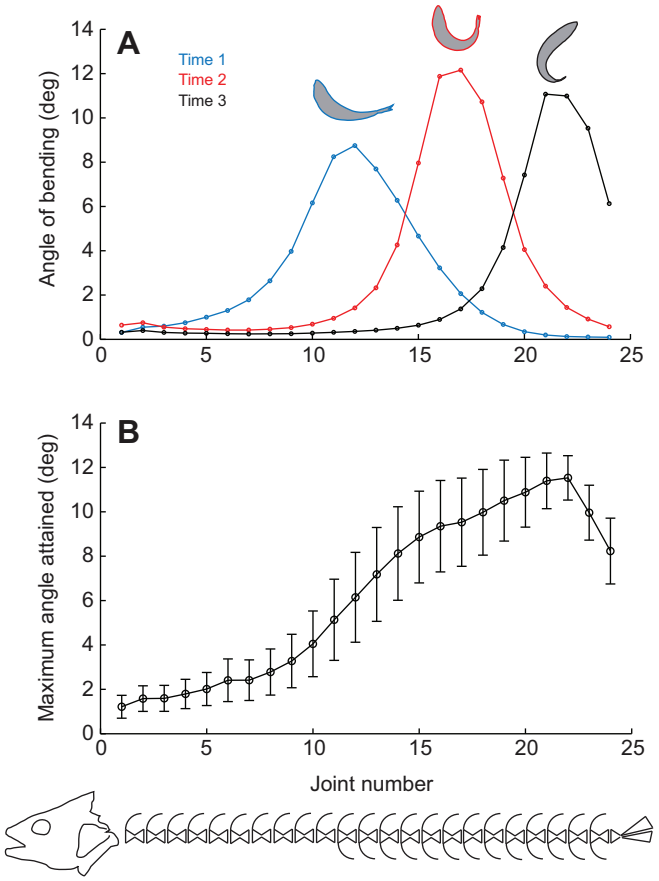

Fig. 4. Pattern I bending. (A) Representative plot of the angle of bending at each intervertebral joint (IVJ) along the length of the fish at each of the three time points evaluated (blue, red and black, respectively). (B) Mean maximum bending angle achieved (±1 s.d.) in pattern I startle responses. These are the maximum angles attained by each IVJ at any time during each startle response (*N*=3 individuals and 10 startle responses, pooled).

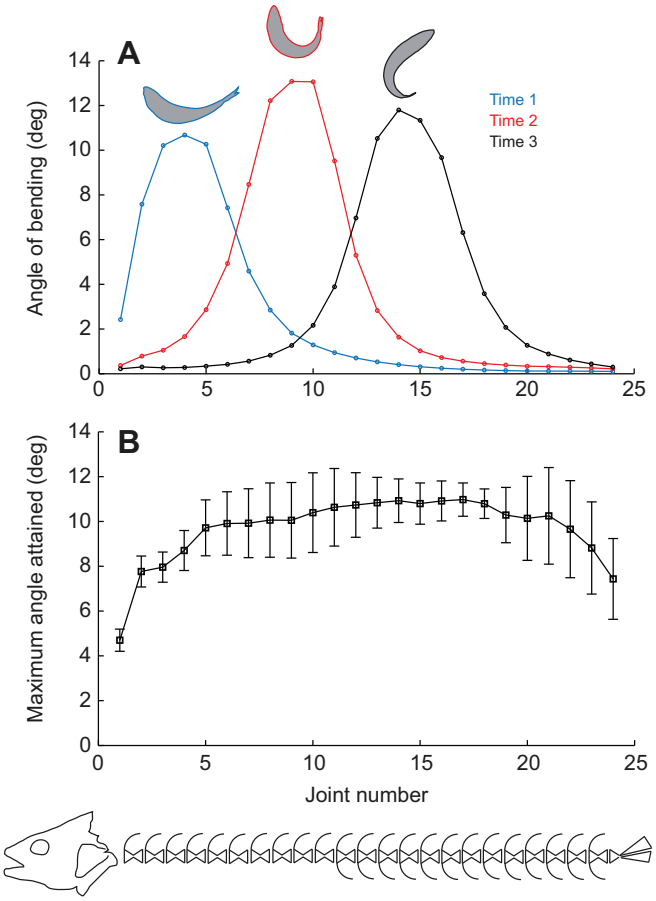

Fig. 5. Pattern II bending. (A) Representative plot of the angle of bending at each IVJ along the length of the fish at each of the three time points evaluated (blue, red and black, respectively). (B) Mean maximum bending angle achieved (±1 s.d.) in pattern II sequences. These are the maximum angles attained by each IVJ at any time during each startle response (*N*=2 individuals and 6 startle responses, pooled).

traveled posteriorly and is localized in the anterior part of the caudal region, centered approximately at IVJs 13–19. Finally, at time 3, this wave of bending continues down the caudal region, while the more rostral regions begin to straighten out as the fish swims or glides away. A representative plot from one individual shows this pattern of bending as it occurs throughout one sequence (Fig. 4A). During pattern I startle responses, the majority of the body bending occurs in the abdominal and caudal regions of the fish, while the cervical region remains relatively straight. Pattern I bending occurred in 10 of the 16 trials across all three individuals.

The *in vivo* range of motion in a pattern I startle response appears to be greater in the caudal joints. The range of motion of each joint, approximated by the mean maximum bending angles (±1 s.d.), indicates greater bending in the caudal region in all three individuals and across the 10 sequences (Fig. 4B). There was no effect of individual on maximum bending angle attained (P=0.0969), thus we pooled the data from these 10 sequences.

In pattern I there was a significant effect (P<0.0001) of region on maximum bending angle attained (Fig. 6). The *post hoc* analysis shows a clear distinction in maximum IVJ angle attained between the cervical and abdominal (P=0.00018), abdominal and caudal (P<0.0001), and cervical and caudal regions (P<0.0001).

The second pattern of bending is characterized by greater bending angles in the more rostral IVJs (Fig. 5A). At time 1, we see substantial bending, up to 10.5 deg, in the cervical region. At time 2, the moment of greatest overall body curvature, bending is localized in the abdominal region, centered approximately at IVJs 6–10. The wave of bending then passes caudally as the fish swims or glides away. While the range of motion in the cervical and abdominal regions is greater in pattern II, the caudal joints remain at ~10–12 deg, similar to the range of motion in the pattern I caudal joints (Fig. 5A). Out of a total of 16 startle responses, pattern II startle responses were observed in six sequences performed by two of the three individuals. There was no effect of individual (P=0.0366), thus we pooled the data from these two individuals.

In pattern II bending there was also a significant effect (P<0.0001) of region on maximum bending angle attained (Fig. 6). The *post hoc* Tukey HSD test showed significant differences between the cervical and abdominal IVJ angles (P=0.0002) and the cervical and caudal IVJ angles (P<0.0001), but there was no significant difference between the abdominal and caudal angles attained (P=0.9987).

3D kinematics

Precision and resolution

The mean standard deviation for the 306 pairwise intermarker distances (unfiltered) from 51 startle responses was 0.22 mm (supplementary material Fig. S1A), and the mean standard deviation from 24 stationary sequences was 0.047 mm (supplementary material

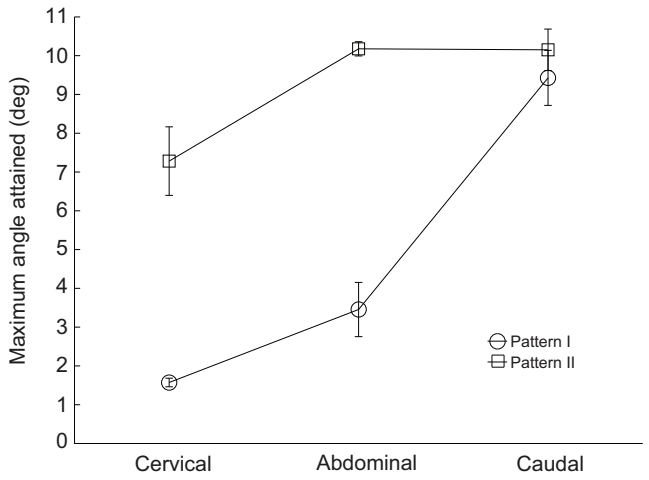

Fig. 6. Comparison between pattern I and pattern II in the three regions of the striped bass vertebral column. Points are the mean maximum angle attained for each region, ± 1 s.d., pooled across sequences.

Fig. S1B). RMSD of rotations and translations in the stationary fish were ~0.5 deg and 0.05 mm, respectively, resulting in peak-to-peak resolution of 0.2–0.3 mm in translation (supplementary material Fig. S2A) and 2–3 deg in rotation (supplementary material Fig. S2B).

Translations

There does not seem to be a clear pattern of translation within the caudal IVJs during the startle response. In the filtered data we saw small displacements occurring throughout the startle response, and no consistent patterns across sequences, such that the results are characteristic of noise. When we calculated the mean translations across all 51 startle responses pooled from the five individuals, we found mediolateral translation of 0.13±0.11 mm, axial translation of 0.19±0.12 mm and dorsoventral translation of 0.18±0.17 mm, all of which were within our estimated resolution of 0.2–0.3 mm.

Rotations

The XROMM results suggest that lateral bending is the primary rotation occurring during the startle response of striped bass. Indeed, we found no consistent pattern of dorsoventral bending or axial rotation during the startle response of the striped bass. When time, polarity of lateral bending and polarity of axial rotation are standardized across the 51 sequences from five individuals, the mean values for dorsoventral bending and axial rotation are close to zero, indicating that the peaks from multiple startle responses cancel each other out (Fig. 7).

In contrast, our results indicate a very clear and consistent pattern of lateral bending (Fig. 7). For a fish initiating a startle response in which the concave side will be the right side of the fish, we see that bending at the caudally located marked vertebrae generally begins with an initial bend toward the left (Fig. 7C). Beyond this point, the marked vertebrae bend towards the right side of the fish. At the transition between stage 1 and stage 2 of the startle response, the marked vertebrae continue the lateral excursion and reach the maximum laterally bent position during stage 2. This overall pattern of lateral bending is consistent across 51 sequences from five individuals, as shown by mean lateral bending with time and polarity standardized (Fig. 7C). This mean waveform retains the slight bend to the left, followed by a bend to the right that peaks in the caudal vertebrae (marked region) well after the stage 1 to stage 2 transition,

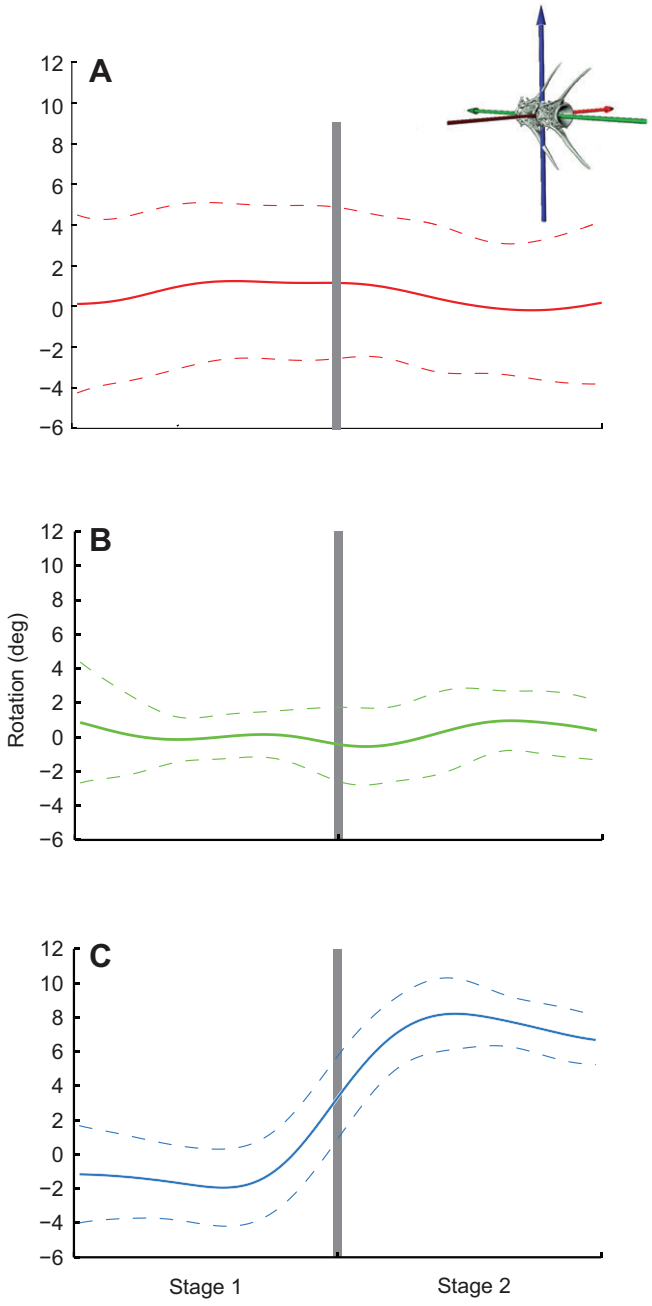

Fig. 7. Mean 3D bending (±1 s.d.) of IVJs across five individuals and 51 startle responses. All sequences were analyzed during stage 1 and stage 2 only. Lateral bending was multiplied by −1 for bends to the left, such that all bends were standardized to be bends toward the right side of the fish. Axial rotation was also multiplied by −1 for bends to the left, but dorsoventral bending was not multiplied by −1. Inset: the joint coordinate system (JCS) used to measure rotations: (A) rotation about the red axis, dorsoventral bending; (B) rotation about the green axis, axial rotation; (C) rotation about the blue axis, lateral bending. Rotation polarity (sign convention) was determined by the right-hand rule with the thumb pointing in the direction of the arrows (inset).

indicating that these are consistent features across sequences and individuals.

Mean maximum lateral bending rotation was 10.41±3.57 deg (N=51 startle responses from five individuals). This value is higher than the apparent mean maximum in Fig. 7C because the maxima

occurred at slightly different times relative to the stage 1–stage 2 transition, so the peaks were smoothed out. This value is not significantly different from the mean maximum lateral bending in the caudal region measured in the 2D study (9.79±0.859 deg, where N=16 startle responses from three individuals).

DISCUSSION

When considered in the context of our previous mechanical testing results, the results of the present study indicate that vertebral column and IVJ tissues of striped bass are quite compliant at IVJ angles observed *in vivo*, and likely do not contribute to whole-body stiffness or elastic energy storage. We identified two patterns of lateral bending that both resulted in maximum angles in each region occurring within the neutral zone of bending described in previous mechanical investigations, such that little stress is experienced about the IVJs.

2D kinematics

A pattern I startle response results in variation along the length of the vertebral column such that the greatest IVJ bending angles occur in the caudal region of the fish (Fig. 4B, Fig. 6). Pattern I is the more common behavior observed, and our finding of greater bending in the caudal region supports what has been previously reported using estimates of midline curvature or indirectly calculated IVJ angles in fishes (Videler and Hess, 1984; Jayne and Lauder, 1995; Donley and Dickson, 2000; Goldbogen et al., 2005; Horner and Jayne, 2008).

For example, maximum midline curvature for the startle response in rainbow trout (*Oncorhynchus mykiss*) was greatest in the caudal region, suggesting that IVJs were bending to a greater degree in that region (Goldbogen et al., 2005). In both kawakawa tuna (*Euthynnus affinis*) and chub mackerel (*Scomber japonicus*), indirect calculations of IVJ bending angles showed the greatest range of motion in the caudal joints, followed by the cervical joints and finally a slightly smaller range of motion in the abdominal region (Donley and Dickson, 2000). Finally, maximum midline curvature increased caudally in largemouth bass (*Micropterus salmoides*), saithe (*Pollachius virens*) and mackerel (*Scomber scombrus*) (Jayne and Lauder, 1995; Videler and Hess, 1984).

However, this result can be quite misleading. Based solely on the pattern I bending behaviors, the cervical region of the fish showed the lowest *in vivo* range of motion, followed by the abdominal region, and finally the caudal region, which had the greatest range of motion (Fig. 4B, Fig. 6). Yet the pattern II bending behaviors reveal a different result. The cervical IVJs bend to a much greater degree in pattern II than in pattern I bends, and the abdominal bending angles in pattern II can be as great as those found in the caudal region (Fig. 5B, Fig. 6). In fact, there is no significant difference between the abdominal and caudal bending angles during the pattern II bends. All the variation occurs between the cervical region and the more posterior joints. Therefore, because of the pattern II bending behavior, we suggest that while the cervical vertebrae have the lowest range of motion relative to the more posterior joints, the *in vivo* range of motion of these cervical IVJs is greater than previously suspected.

3D kinematics

The results of the present study indicate that the kinematics of adjacent caudal vertebrae during the startle response are primarily restricted to lateral bending, within our limited ability to measure other degrees of freedom. The mediolateral, axial and dorsoventral translations generally fell within the estimated 0.2–0.3 mm measurement resolution of our system (supplementary material Figs S1, S2). The lack of a consistent pattern of dorsoventral and axial rotation during the startle response results in mean values across the 51 sequences that cancel each other out (Fig. 7A,B). The mean values for these rotations are between 1 and 2 deg, and therefore fall below the resolution of the current study (supplementary material Fig. S2).

Although the present study was not able to resolve dorsoventral bending and axial rotations, it is important to note that these rotations cannot be conclusively discounted. The data suggest that dorsoventral and axial rotations up to 3 deg in magnitude may occur, and these small rotations are worthy of further investigation. If rotations of 2–3 deg occur at even the last 8–10 IVJs, the resulting angle of attack of the caudal fin may be substantial enough to account for the ~15 and 30 deg rotation associated with the asymmetry of the caudal fin stroke reported in bluegill sunfish and sturgeon, respectively (Lauder, 2000).

We were somewhat disappointed that the dorsoventral and axial rotation resolution was not sufficient to measure the small rotations that likely occur about these axes, but in retrospect, this study challenged the XROMM system in almost every possible way. Water absorbs X-rays, so recording aquatic animals is always a challenge. Recording in two planes is even more difficult because it is necessary to orient the X-ray beams obliquely, which increases the distance that the beams must penetrate the water (Fig. 2B). To minimize this effect we oriented the beams at 60 deg to each other, but that then reduces the resolution relative to 90 deg. X-ray energies were at near-maximum for the machines (100 kV and 200 mA), and still we were not able to use a short enough exposure time to prevent motion artifacts (supplementary material Figs S1, S2). This motion likely accounted for the lower marker tracking precision (mean of 0.22 mm) relative to other XROMM studies, including an aquatic feeding study, in which precisions were in the 0.04–0.08 mm range (Brainerd et al., 2010; Dawson et al., 2011; Gidmark et al., 2012). In addition, the need to use the smallest volume of water possible in the tank to optimize X-ray contrast may potentially create a physical limitation of its own. It is possible that the water level confined the fish to C-starts primarily performed using lateral bending. Unfortunately, because of the complications with using additional water, we were not able to account for this limitation. It should be noted that it is possible that dorsoventral and axial rotations may increase in magnitude if the animals are less restricted in the experimental tank. Finally, the small size and surgical inaccessibility of the vertebrae in this study meant that distances between the markers on each vertebra were typically about 5–7 mm, which, combined with the low marker tracking precision, substantially reduced the resolution of the rigid body animations. In general, for better resolution, markers should be placed at least 10 mm apart, at least four markers per bone should be used, and they should be as non-coplanar as possible (Miranda et al., 2011).

However, the accuracy was sufficient to resolve the larger lateral bending angles. The pattern of lateral bending across all five individuals in the present study was highly consistent. In each sequence, lateral bending occurred at the caudally located marked vertebrae towards the end of stage 1. The vertebrae continued to bend through the point of greatest body curvature, with peak lateral excursion reached during stage 2 (Fig. 7C). The mean maximum lateral bending angle was 10.4 deg, which is not significantly different from the mean maximum lateral bending angle (9.79 deg) measured for the caudal region of the striped bass during the 2D investigation of the present study. As there were no surgeries performed in the 2D lateral bending investigation, this result

provides evidence that the fish were able to recover from the invasive surgery performed in the XROMM experiments. Additionally, this lateral bending angle of 10 deg is greater than that reported between adjacent vertebrae in the bluegill sunfish (*L. macrochirus*) and in muskellunge (*Esox masquinongy*) and is similar to the bending angles reported for various teleost fish species (Jayne and Lauder, 1993; Brainerd and Patek, 1998; Hale, 2002).

Functional implications

Our previous *in vitro* mechanical testing results and current *in vivo* kinematics indicate that the vertebral column of the striped bass is quite compliant. In fact, Fig. 8 shows that very little moment is generated about the joints during even the largest IVJ angles measured during startle responses. If we plot the largest magnitude rotations measured in the present experiment on the force–displacement curves generated in our previous mechanical testing experiment, all the angles occur within the neutral zone of bending (Fig. 8). This is relevant to steady swimming, as the startle response should result in the greatest bending angles achieved *in vivo*. These results suggest that the soft tissues of the IVJs experience very little stress during both steady swimming and escape behaviors in these fish. Therefore, the vertebral column's contributions to whole-body stiffness in striped bass should be minimal.

In addition, there is little evidence to suggest that the vertebral column plays a substantial role in swimming energetics. Several studies have suggested that the vertebral column of fish acts in a spring-like manner providing elastic recoil that aids swimming energetics (Rockwell et al., 1938; Nursall, 1958; Fierstine and Walters, 1968; Symmons, 1979; Long, 1992; Videler, 1993). Other studies have countered this idea, suggesting that the vertebral column plays a purely mechanical role during swimming (Hebrank, 1982; Hebrank et al., 1990). The results of our mechanical and kinematic experiments are in agreement with the latter argument. Allowing the IVJs to operate near failure and at 60% resilience, as measured previously in striped bass (Nowroozi and Brainerd, 2012), we estimate the maximum energy returned to the system to be 0.024 J (summed across all 24 IVJs). Assuming a similar fast muscle power output to the 35 W kg^{-1} measured in the short horned sculpin (Altringham and Johnston, 1990), this 0.024 J results in just 0.5% of the 17.5 W of power required by a 0.5 kg fish. This value decreases substantially when we input the actual IVJ angles measured in the present study. For example, in the cervical region, maximum bending angles of ~9 deg result in 0.002 N m of moment about each joint, returning 1.9×10^{-4} J of energy to the system. Similarly, the abdominal region returns 6.9×10^{-4} J and the caudal region 3.8×10^{-4} J of energy. Even at the high frequencies of the startle response, these values result in a maximum of 0.06% per IVJ (1.4% for the entire vertebral column) of the 17.5 W of muscle power required during burst swimming. Thus, it is unlikely that the vertebral column provides substantial spring-like recoil to the system.

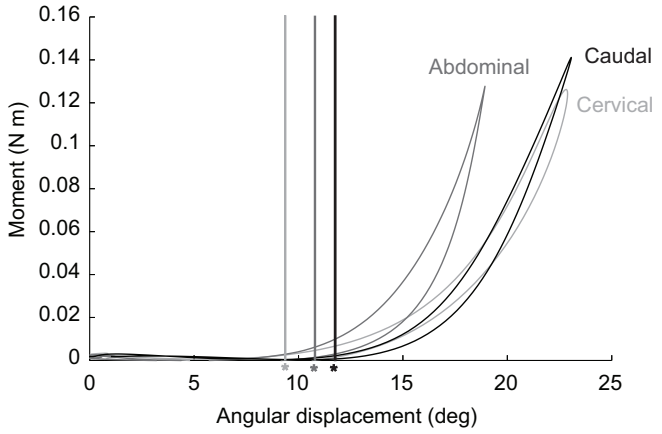

Fig. 8. Typical moment–displacement curve for the cervical (light gray), abdominal (dark gray) and caudal (black) regions with maximum bending angles for each region indicated by asterisks (modified from Nowroozi and Brainerd, 2012).

It is important to note that that these performance results may be quite species specific. Previous mechanical testing studies have shown that while a large neutral zone is present in some species, including the longnose gar and the striped bass (Long et al., 1996; Nowroozi and Brainerd, 2012), there are other species such as skipjack tuna and blue marlin that do not exhibit a neutral zone at all (Hebrank, 1982; Hebrank et al., 1990; Long, 1992). Thus, in these species it is possible that significant stress is developed about the IVJs, thereby contributing to body stiffness and possibly to swimming energetics.

More generally, the presence of neutral zones has been explored in mammals as well, and similar variability both within an individual and between species has been observed. Mechanical testing of the intervertebral joints of the rabbit, badger, seal, rat and human resulted in significant neutral zones (Yamamoto et al., 1989; Gal, 1993a; Gal, 1993b; Kettler et al., 2004; Panjabi et al., 2001). Within these species, lumbosacral neutral zones were identified for the rabbit, badger, seal and human, while lumbar–lumbar neutral zones were only found for the rabbit, seal and human (Yamamoto et al., 1989; Gal, 1993a; Kettler et al., 2004). Additionally, cervical neutral zones were reported for humans, and substantial variation within that region alone was found. Moreover, variation in cervical neutral zones varied greatly depending on the axis of rotation (Panjabi et al., 2001). Finally, neutral zones were not found in investigations of the dolphin, tiger, sheep or monkey intervertebral joints (Gal, 1993a; Gal, 1993b; Long et al., 1997). Therefore, to clearly understand the role of the vertebral column and IVJs in locomotor performance it is imperative to combine kinematic studies with studies of mechanical testing that span regions of the vertebral column and explore all applicable axes of rotation. In combination, these mechanical and kinematic studies will offer a more clear understanding of the locomotor function of the vertebral column than either study can offer alone.

Finally, small translations, dorsoventral rotations and axial rotations all suggest that the movement between vertebrae can be explained primarily by lateral bending about the origin of our JCS. This would suggest that the axis of rotation between the two adjacent vertebrae lies directly in the center of the joint. This result is in accordance with previous studies that model the swimming fish as a homogeneous bending beam with its neutral axis of bending running directly through the midline of the vertebral column (Alexander, 1969; Lighthill, 1971; Long and Nipper, 1996; Cheng et al., 1998; Goldbogen et al., 2005).

ACKNOWLEDGEMENTS

We thank Susquehanna Aquaculture for providing the animals for this study. We thank Erika Giblin for help with animal surgery and data collection; Kia Huffman for help with data collection; Eric LoPresti, Jimmy Tarrant and Nicholas Gidmark for help with housing and husbandry; Christen Dillard for help with digitizing videos; Dale Ritter for helpful discussions regarding marker implantation; and Nicole Danos and Doug Morse for access to CT scanners. Steve Gatesy, Thomas Roberts, Sharon Swartz, John Long, Manny Azizi, David Baier, Ariel Camp, Caroline Harper and the Morphology Group at Brown provided helpful discussion and suggestions for the manuscript.

AUTHOR CONTRIBUTIONS

Both authors contributed significantly to the conception, experimental design, execution, analysis, drafting and revision of the present study and publication.

COMPETING INTERESTS

No competing interests declared.

FUNDING

This work was supported by grants from the W. M. Keck Foundation and the National Science Foundation [grant nos 0552051, 0629372 and 0840950] to E.L.B. and from the Bushnell Research and Education Fund to B.N.N.

REFERENCES

Alexander, R. M. (1969). The orientation of muscle fibers in the myomeres of fishes. *J. Mar. Biol. Assoc. U. K.* **49**, 263-290.
Altringham, J. D. and Johnston, I. A. (1990). Modelling muscle power output in a swimming fish. *J. Exp. Biol.* **148**, 395-402.
Brainerd, E. L. and Patek, S. N. (1998). Vertebral column morphology, C-start curvature, and the evolution of mechanical defenses in tetraodontiform fishes. *Copeia* 4, 971-984.
Brainerd, E. L., Baier, D. B., Gatesy, S. M., Hedrick, T. L., Metzger, K. A., Gilbert, S. L. and Crisco, J. J. (2010). X-ray reconstruction of moving morphology (XROMM): precision, accuracy and applications in comparative biomechanics research. *J. Exp. Zool. A* **313**, 262-279.
Cheng, J. Y., Pedley, T. J. and Altringham, J. D. (1998). A continuous dynamic beam model for swimming fish. *Philos. Trans. R. Soc. B* **353**, 981-997.
Dawson, M. M., Metzger, K. A., Baier, D. B. and Brainerd, E. L. (2011). Kinematics of the quadrate bone during feeding in mallard ducks. *J. Exp. Biol.* **214**, 2036-2046.
Donley, J. M. and Dickson, K. A. (2000). Swimming kinematics of juvenile kawakawa tuna (*Euthynnus affinis*) and chub mackerel (*Scomber japonicus*). *J. Exp. Biol.* **203**, 3103-3116.
Fierstine, H. L. and Walters, V. (1968). Studies in locomotion and anatomy of scombroid fishes. In *Memoirs of the Southern California Academy of Sciences*, Vol. 6, pp. 1-31. Los Angeles, CA: Southern California Academy of Sciences.
Gál, J. M. (1993a). Mammalian spinal biomechanics. I. Static and dynamic mechanical properties of intact intervertebral joints. *J. Exp. Biol.* **174**, 247-280.
Gal, J. M. (1993b). Mammalian spinal biomechanics. II. Intervertebral lesion experiments and mechanisms of bending resistance. *J. Exp. Biol.* **174**, 281-297.
Gidmark, N. J., Staab, K. L., Brainerd, E. L. and Hernandez, L. P. (2012). Flexibility in starting posture drives flexibility in kinematic behavior of the kinethmoid-mediated premaxillary protrusion mechanism in a cyprinid fish, *Cyprinus carpio*. *J. Exp. Biol.* **215**, 2262-2272.
Goldbogen, J. A., Shadwick, R. E., Fudge, D. S. and Gosline, J. M. (2005). Fast-start muscle dynamics in the rainbow trout *Oncorhynchus mykiss*: phase relationship of white muscle shortening and body curvature. *J. Exp. Biol.* **208**, 929-938.
Govett, P. D., Olby, N. J., Marcellin-Little, D. J., Rotstein, D. S., Reynolds, T. L. and Lewbart, G. A. (2004). Stabilisation of scoliosis in two koi (*Cyprinus carpio*). *Vet. Rec.* **155**, 115-119.
Gray, A. (1993). *Modern Differential Geometry of Curves and Surfaces*. Boca Raton, FL: CRC Press.
Hale, M. E. (2002). S- and C-start escape responses of the muskellunge (*Esox masquinongy*) require alternative neuromotor mechanisms. *J. Exp. Biol.* **205**, 2005-2016.
Harms, C. A. (2005). Surgery in fish research: common procedures and postoperative care. *Lab Anim. (NY)* **34**, 28-34.
Hebrank, M. R. (1982). Mechanical properties of fish backbones in lateral bending and in tension. *J. Biomech.* **15**, 85-89.
Hebrank, J. H., Hebrank, M. R., Long, J. H., Block, B. A. and Wainwright, S. A. (1990). Backbone mechanics of the blue marlin *Makaira nigricans* (Pisces, Istiophoridae). *J. Exp. Biol.* **148**, 449-459.
Horner, A. M. and Jayne, B. C. (2008). The effects of viscosity on the axial motor pattern and kinematics of the African lungfish (*Protopterus annectens*) during lateral undulatory swimming. *J. Exp. Biol.* **211**, 1612-1622.
Jayne, B. C. and Lauder, G. V. (1993). Red and white muscle activity and kinematics of the escape response of the bluegill sunfish during swimming. *J. Comp. Physiol. A* **173**, 495-508.
Jayne, B. C. and Lauder, G. V. (1995a). Speed effects on midline kinematics during steady undulatory swimming of largemouth bass, *Micropterus salmoides*. *J. Exp. Biol.* **198**, 585-602.
Kettler, A., Marin, F., Sattelmayer, G., Mohr, M., Mannel, H., Dürselen, L., Claes, L. and Wilke, H. J. (2004). Finite helical axes of motion are a useful tool to describe the three-dimensional in vitro kinematics of the intact, injured and stabilised spine. *Eur. Spine J.* **13**, 553-559.
Lauder, G. V. (2000). Function of the caudal fin during locomotion in fishes: kinematics, flow visualization, and evolutionary patterns. *Am. Zool.* **40**, 101-122.
Lewbart, G. A. and Harms, C. (1999). Building a fish anesthesia delivery system. *Exotic DVM* **1**, 25-28.
Lighthill, M. J. (1971). Large-amplitude elongated-body theory of fish locomotion. *Proc. R. Soc. B* **179**, 125-138.
Long, J. H. (1992). Stiffness and damping forces in the intervertebral joints of blue marlin (*Makaira nigricans*). *J. Exp. Biol.* **162**, 131-155.
Long, J. H. (1998). Muscles, elastic energy, and the dynamics of body stiffness in swimming eels. *Am. Zool.* **38**, 771-792.
Long, J. H. and Nipper, K. S. (1996). The importance of body stiffness in undulatory propulsion. *Am. Zool.* **36**, 678-694.
Long, J. H., McHenry, M. J. and Boetticher, N. C. (1994). Undulatory swimming: How traveling waves are produced and modulated in sunfish (*Lepomis gibbosus*). *J. Exp. Biol.* **192**, 129-145.
Long, J. H., Hale, M. E., McHenry, M. J. and Westneat, M. W. (1996). Functions of fish skin: flexural stiffness and steady swimming of longnose gar, *Lepisosteus osseus*. *J. Exp. Biol.* **199**, 2139-2151.
Long, J. H., Jr, Pabst, D. A., Shepherd, W. R. and McLellan, W. A. (1997). Locomotor design of dolphin vertebral columns: bending mechanics and morphology of *Delphinus delphis*. *J. Exp. Biol.* **200**, 65-81.
Long, J. H., Adcock, B. and Root, R. (2002). **G**. (2002). Force transmission via axial tendons in undulating fish: a dynamic analysis. *Comp. Biochem. Physiol.* **133**, 911-929.
Long, J. H., Koob-Emunds, M. and Koob, T. J. (2004). The mechanical consequences of vertebral centra. *Bull. Mt. Desert Isl. Biol. Lab.* **43**, 99-101.
McHenry, M. J., Pell, C. A. and Jr, J. (1995). Mechanical control of swimming speed: stiffness and axial wave form in undulating fish models. *J. Exp. Biol.* **198**, 2293-2305.
Miranda, D. L., Schwartz, J. B., Dawson, M. M., Fleming, B. C. and Crisco, J. J. (2011). *Markerless Tracking Error of a Biplanar X-Ray Motion Capture System.* American Society of Biomechanics, 35th Annual Meeting, Long Beach, California, 10-13 August, 2011.
Nelson, J. S. (1994). *Fishes of the World*, 4th edn. New York, NY: Wiley-Interscience.
Nowroozi, B. N. and Brainerd, E. L. (2012). Regional variation in the mechanical properties of the vertebral column during lateral bending in *Morone saxatilis*. *J. R. Soc. Interface* **9**, 2667-2679.
Nowroozi, B. N., Harper, C. J., De Kegel, B., Adriaens, D. and Brainerd, E. L. (2012). Regional variation in morphology of vertebral centra and intervertebral joints in striped bass, *Morone saxatilis*. *J. Morphol.* **273**, 441-452.
Nursall, J. R. (1958). The caudal fin as a hydrofoil. *Evolution* **12**, 116-120.
Panjabi, M. M., Crisco, J. J., Vasavada, A., Oda, T., Cholewicki, J., Nibu, K. and Shin, E. (2001). Mechanical properties of the human cervical spine as shown by three-dimensional load-displacement curves. *Spine* **26**, 2692-2700.
Rockwell, H., Evans, F. G. and Homer, C. P. (1938). The comparative morphology of the vertebrate spinal column. Its form as related to function. *J. Morphol.* **63**, 87-117.
Rousseau, M. A., Ulrich, J. A., Bass, E. C., Rodriguez, A. G., Liu, J. J. and Lotz, J. C. (2007). Stab incision for inducing intervertebral disc degeneration in the rat. *Spine* **32**, 17-24.
Schmitz, R. J. (1995). Ultrastructure and function of cellular components of the intercentral joint in the percoid vertebral column. *J. Morphol.* **226**, 1-24.
Symmons, S. (1979). Notochordal and elastic components of the axial skeleton of fishes and their functions in locomotion. *J. Zool.* **189**, 157-206.
Videler, J. J. (1993). *Fish Swimming*. London: Chapman & Hall.
Videler, J. J. and Hess, F. (1984). Fast continuous swimming of two pelagic predators, saithe (*Pollachius virens*) and mackerel (*Scomber scombrus*): a kinematic analysis. *J. Exp. Biol.* **109**, 209-228.
Wainwright, S. A., Vosburgh, F. and Hebrank, J. H. (1978). Shark skin: function in locomotion. *Science* **202**, 747-749.
Weihs, D. (1973). The mechanism of rapid starting of slender fish. *Biorheology* **10**, 343-350.
Westneat, M. W., Hoese, W., Pell, C. and Wainwright, S. (1993). The horizontal septum: mechanisms of force transfer in locomotion of scombrid fishes (Scombridae, Perciformes). *J. Morphol.* **217**, 183-204.
Wilke, H. J., Wenger, K. and Claes, L. (1998). Testing criteria for spinal implants: recommendations for the standardization of in vitro stability testing of spinal implants. *Eur. Spine J.* **7**, 148-154.
Yamamoto, I., Panjabi, M. M., Crisco, T. and Oxland, T. (1989). Three-dimensional movements of the whole lumbar spine and lumbosacral joint. *Spine* **14**, 1256-1260.

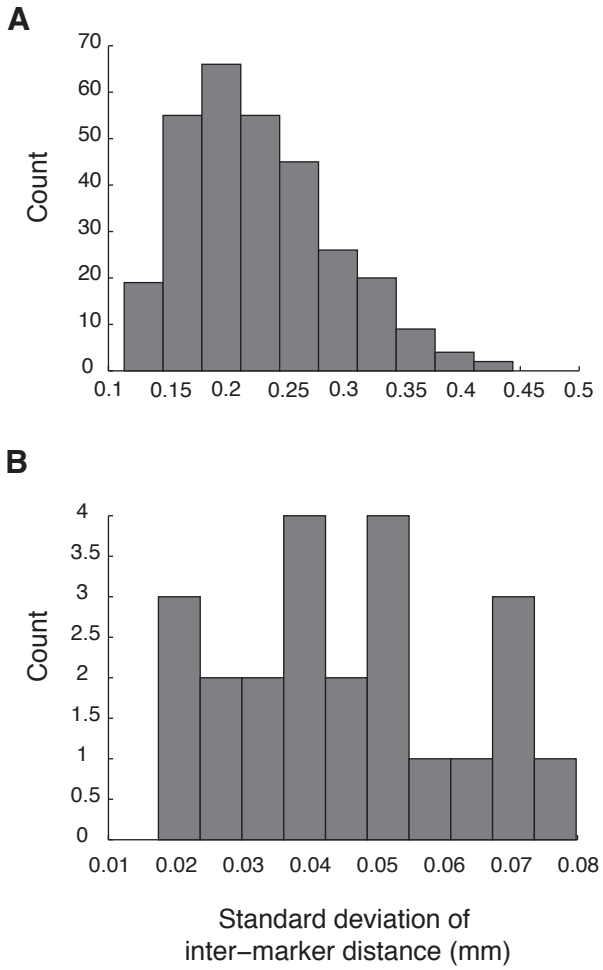

Figure S1. Precision of 3D marker tracking during *in vivo* measurement conditions. (A) Histogram of the standard deviation of 306 intermarker distances from 51 startle response sequences. The mean standard deviation is 0.22 mm. (B) Histogram of the standard deviation of 24 intermarker distances from four stationary sequences. The mean standard deviation is 0.047 mm. Note that the mean standard deviation is approximately five times greater during the startle response. This decreased precision is likely due to motion artifacts. Unfortunately, the difficulty in visualizing markers through the large amount of water limited us to an exposure time of 500μs, which was not sufficient to remove all motion blur.

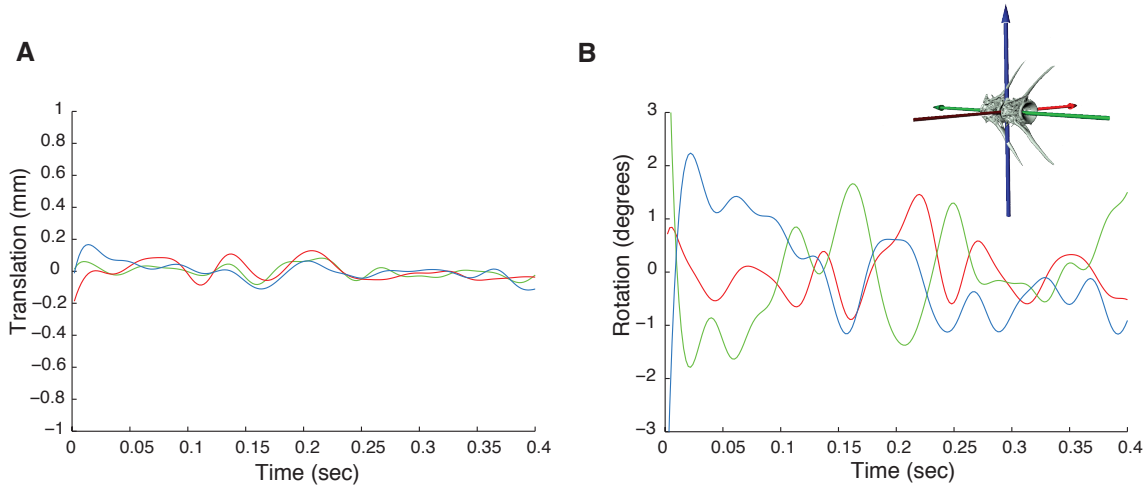

Figure S2. Root Mean Square Deviation (RMSD) of one representative stationary sequence portraying (A) translations and (B) rotations. Since the fish are stationary we expect these RMSD values to be zero. Mean RMSD translations for the four stationary sequences were indeed quite small: 0.05 mm mediolateral translation (red); 0.03 mm axial translation (green); and 0.04 mm dorsoventral translation resulting in peak-to-peak translations of 0.2-0.3 mm translational resolution. Mean RMSD rotations for the four stationary sequences: 0.45˚ for dorsoventral rotation (red); 0.52˚ for axial rotation (green); and 0.48˚ for lateral bending (blue) resulting in peak-to-peak rotations in a stationary fish of up to 2-3˚ rotational resolution.

Movie S1. Dorso-ventral camera view of *M. saxatilis* performing a startle response. The subject begins positioned with cranial towards the left of the screen and caudal towards the right of the screen. Video was captured at 500 frames s^{-1}, 500 µs exposure time, 70 kV X-ray voltage and 320 mA of X-ray current. It is important to note that as the water depth is disturbed, first by the stimulus and later by the movements of the fish, the exposure of those regions changes, causing more shallow areas to become temporarily brighter and deeper areas to become temporarily darker.